

# Phenomenological Local Potentials for $\pi^- + {}^{12}\text{C}$ Scattering from 120 to 766 MeV

S. W. Hong<sup>\*†</sup> and B. T. Kim<sup>\*</sup>

<sup>\*</sup>Department of Physics and Institute of Basic Science, Sungkyunkwan University  
Suwon 440-746, Republic of Korea

<sup>†</sup>TRIUMF, 4004 Wesbrook Mall, Vancouver, B.C. Canada, V6T 2A3

## Abstract

Pion-nucleus scattering cross sections are calculated by solving a Schrödinger equation reduced from the Klein-Gordon equation. Local potentials are assumed, and phenomenological potential parameters are searched energy-dependently for  $\pi^- + {}^{12}\text{C}$  system so as to reproduce not only elastic differential cross sections but also total elastic, reaction and total cross sections at 13 pion incident energies from 120 to 766 MeV. The real and imaginary parts of the local potentials thus obtained are shown to satisfy the dispersion relation. The imaginary part of the potentials as a function of the pion energy is found to peak near the  $\Delta(1232)$ -resonance energy. The strong absorption radius of the pion projectile with incident energies near the  $\Delta$ -resonance region is found to be about  $1.6A^{1/3}$  fm, which is consistent with previous studies of the region where the decay of the  $\Delta$ 's takes place in nuclei. The phenomenological local potentials are then compared with the local potentials exactly phase-shift equivalent to Kisslinger potentials for pion energies near the  $\Delta$ -resonance.

PACS number: 24.10.Ht, 25.40.Ny, 25.80.Dj

# 1 Introduction

For the last two decades, pion-nucleus elastic scattering has been studied by a number of people using a variety of theoretical methods, some of which are given in Refs. [1 – 16]. The aim of most theoretical works is to understand the pion-nucleus scattering and thereby the nuclear structure in the framework of the multiple scattering theory by using elementary pion-nucleon scattering amplitudes obtained from the pion-nucleon scattering data. Normally, the Klein-Gordon equation is solved either in coordinate space [3, 4] or in momentum space [5, 6] with various forms of elementary t-matrices including nuclear structure effects [1 – 12]. There are also works using approaches other than directly solving the Klein-Gordon equation, such as the  $\Delta$ -isobar model [13, 14, 15] taking into account production and propagation of the  $\Delta$ -isobar in nuclei. Though numerous works, essentially solving the Klein-Gordon equation in different ways, have revealed much of pion-nucleus dynamics, the understanding of the pion-nucleus scattering is still not quite satisfactory.

On the other hand, when one tries to do a quantitative calculation of cross sections for a reaction involving pions, such as  $(\pi, \pi')$  or  $(\pi, K)$ , by using the distorted wave Born approximation (DWBA) or the distorted wave impulse approximation (DWIA), it is essential to have the pion distorted wave functions. Even if the accurate pion distorted wave functions may not be achieved, it would be convenient to have a way of treating the distortion effects in a simple manner. The present study was motivated by such a need of the distorted wave functions that could reproduce the pion scattering data by all means so that the distortion effects could be treated.

The optical potentials normally used in the Klein-Gordon equation for the pion-nucleus scattering are known to be nonlocal, particularly in the  $\Delta$ -resonance region due to the  $P$ -wave nature of the resonance. However, it would be not only easier to visualize but also interesting if one can localize the nonlocal potential and look at the dynamics of the scattering from a different point of view. Recently, Satchler [16] showed a method of

reducing the Klein-Gordon equation into the form of a Schrödinger equation by redefining some kinematical quantities. He then reproduced not only elastic but also inelastic differential cross sections of the pion near the  $\Delta(1232)$ -resonance energy for various target nuclei ranging from  $^{40}\text{Ca}$  to  $^{208}\text{Pb}$  by using local potentials of the Woods-Saxon form. In Section 2 we follow Satchler, reduce the Klein-Gordon equation to a Schrödinger equation, and search for phenomenological local optical potentials which can reproduce the scattering data.

We choose the system of  $\pi^- + ^{12}\text{C}$ , because for this system many experimental data are available in a wide range of energies, 120 - 766 MeV [17, 18, 19] and we are interested in examining the energy-dependency of the pion-nucleus local potentials. We employ the Woods-Saxon form of the local potential [16] and search for the potential parameters to fit the experimental data. The real and imaginary parts of the resulting local potentials are found to be consistent with the dispersion relation. The energy-dependency of the phenomenological local potential shows that the imaginary part of the potential peaks near the  $\Delta$ -resonance energy, and it can be explained by the decay of the  $\Delta$ 's in the nuclear medium, which is manifested as absorption of the pion projectile in the scattering.

We then compare in Section 3 our phenomenological local potential with the local potential exactly phase-shift equivalent to the Kisslinger potential obtained by using the Krell-Ericson transformation method [20], which has been used for instance by Parija [21] and recently by Johnson and Satchler [22]. Section 4 summarizes the paper.

## 2 Phenomenological Local Potentials

### 2.1 The Model

In most works dealing with solving the Klein-Gordon equation, a so-called truncated Klein-Gordon equation is used, which means terms quadratic in the potentials are neglected compared to the pion energy. Then one gets

$$\left[ -(\hbar c)^2 \nabla^2 + 2\omega(V_N + V_C) \right] \phi = (\hbar k c)^2 \phi, \quad (1)$$

where  $\phi$  is the distorted wave function for the relative motion between the pion and the target nucleus,  $V_C$  and  $V_N$  are the Coulomb and the nuclear potentials, respectively, and  $k$  is the relativistic center-of-mass momentum of the pion. In regarding Eq. (1) as the equation for the scattering between the pion and the target nucleus, Stricker, McManus and Carr [4] defined  $\omega$  by

$$\omega = \frac{M_\pi m_T c^2}{M_\pi + m_T}, \quad (2)$$

where  $m_T$  is the target mass given by the target mass number multiplied by the atomic mass unit and  $M_\pi$  is the total energy of the pion in the pion-nucleus center-of-mass system. Satchler then introduced a reduced mass  $\mu$  defined by  $\mu = \omega/c^2$  and put Eq. (1) into the form of a Schrödinger equation

$$\left[ -\frac{\hbar^2}{2\mu} \nabla^2 + V_N + V_C \right] \phi = E_{c.m.} \phi \quad (3)$$

for the scattering of two masses,  $M_\pi$  and  $m_T$  with a center-of-mass kinetic energy  $E_{c.m.} = (\hbar k)^2/2\mu$ . (The incident pion bombarding energy was modified so that a standard nonrelativistic optical model computer program could be used [16].) In what follows, we use this method of solving Eq. (3) with phenomenological Woods-Saxon local potentials.

## 2.2 Results for Phenomenological Local Potentials

The Woods-Saxon form of  $V_N$  in Eq. (3) can be written as

$$V_N(r) = \frac{V}{1 + \exp(X_V)} + i \frac{W}{1 + \exp(X_W)} \quad (4)$$

with

$$X_i = (r - R_i)/a_i, \quad R_i = r_i A^{1/3} \quad (i = V, W),$$

where  $r_i$  and  $a_i$  are radius and diffuseness parameters, respectively, and  $A$  is the target mass number. The Coulomb potential  $V_C$  is given in a simple form obtained from a uniform charge distribution of radius  $R_C = 1.2A^{1/3}$  fm. There are 6 adjustable parameters

in Eq. (4). We fixed them by using a  $\chi^2$ -fitting method. The  $\chi^2$ , written explicitly as

$$\chi^2 = \frac{1}{N} \sum_{i=1}^N \left[ \frac{\sigma_{ex}^i - \sigma_{th}^i}{\Delta\sigma_{ex}^i} \right]^2 \quad (5)$$

is evaluated at each energy, and the potential parameters are adjusted so as to minimize the  $\chi^2$ . In Eq. (5),  $\sigma_{ex}^i$ 's ( $\sigma_{th}^i$ 's) and  $\Delta\sigma_{ex}^i$ 's are the experimental (theoretical) cross sections and uncertainties, respectively, and  $N$  is the number of data used in the fitting. Since experimental total elastic ( $\sigma_E$ ), reaction ( $\sigma_R$ ) and total ( $\sigma_T$ ) cross sections were also available at all energies except for 400 and 500 MeV, we used not only differential cross sections but also  $\sigma_E$ ,  $\sigma_R$  and  $\sigma_T$  as the data,  $\sigma_{ex}^i$ , to be fitted.

In searching for the parameters we first kept the radius parameters,  $r_i$ , as 0.9 or 1.0 fm and the diffuseness parameters,  $a_i$ , as 0.4 or 0.5 fm. When we could not get good fits to the data with these fixed parameters, we let them vary. We tried to find both repulsive and attractive potentials at all energies. It was possible to find attractive potentials at all energies considered here, but repulsive potentials were obtained only at 230, 260 and 280 MeV, which are just above the  $\Delta$ -resonance energy. Satchler also obtained a repulsive Woods-Saxon potential for  $\pi^\pm + {}^{208}\text{Pb}$  at 291 MeV, whereas at other (lower) energies he found attractive potentials [16]. At these 3 energies the cross sections calculated with attractive potentials were indistinguishable from the ones calculated with repulsive potentials. However, one may normally expect a repulsive potential above the resonance. Also, the dispersion relation calculations to be discussed in the next subsection prefer repulsive real potentials just above the  $\Delta$ -resonance energy. Thus, we shall henceforth include in our discussion only repulsive potentials at 230, 260 and 280 MeV. (At energies higher than the  $\Delta$ -resonance there exist several  $N^*$  resonances, but these resonances are not so pronounced as the  $\Delta$ , and they overlap with each other due to broad widths. Indeed, at other energies we could not find repulsive potentials.)

There is a well-known ambiguity in determining the optical potential parameters [16, 23, 24]. Due to the strong absorption taking place in the nuclear surface region, different potentials can often fit the scattering data equally well as long as they have similar values

near the surface region. Actually, we found that when we used only the elastic differential cross sections as the data to be fitted, the extracted potential parameters could not always reproduce the experimental total elastic ( $\sigma_E$ ), reaction ( $\sigma_R$ ) and total ( $\sigma_T$ ) cross sections. However, when we included in the fitting  $\sigma_E$ ,  $\sigma_R$  and  $\sigma_T$  as the data to be reproduced in addition to the differential cross section, the resulting potential parameters reproduced all the cross sections quite well as shown in Figs. 1 and 2. (In Figs. 1 and 2, the experimental data for the pion kinetic energies,  $E = 120 - 280$  MeV and  $E = 486, 584, 663$  and  $766$  MeV are taken from Refs. [17] and [18], respectively. Recently, differential elastic cross section data at  $E = 400$  and  $500$  MeV became available from Ref. [19].) The searched parameters and the  $\chi^2$ -values for each energy are listed in Table 1. The fits to the experimental cross sections are in general very good. But there is some discrepancy in the differential cross sections at low bombarding energies, particularly at  $E = 150$  MeV. At this energy the second minimum of the differential cross section was not reproduced correctly, and the third maximum was underestimated. When we tried to reproduce the data at larger angles by further adjusting the potential parameters, it was possible to fit the larger angle data, but then the first minimum was not reproduced at the right angle. This may be due to that we have used the Woods-Saxon potentials whereas more realistic potentials such as local potentials phase-shift equivalent to Kisslinger potentials [20, 21, 22] look considerably different from the Woods-Saxon form, particularly inside the nucleus, as will be shown in Section 3. However, we also note that similar discrepancies between the calculated and the experimental cross sections at  $E = 150$  MeV can be seen from Refs. [15] and [25], in which the  $\Delta$ -isobar model and the Kisslinger potential are used, respectively.

### 2.3 Dispersion Relation and Discussion

Because the extracted potentials have an ambiguity as mentioned above, it is worthwhile to check whether they satisfy the dispersion relation, which is known to be satisfied by the

real and imaginary parts of the optical potentials [24]. Also, since the relativistic Klein-Gordon equation, normally solved with nonlocal potentials, is reduced to a nonrelativistic Schrödinger equation, it would be interesting to see whether the phenomenological local potentials are consistent with the dispersion relation. The relation is often written in the form of a so-called subtracted dispersion relation as

$$V(E, r) = V(E', r) + \frac{E - E'}{\pi} P \int_0^\infty dE'' \frac{W(E'', r)}{(E'' - E')(E'' - E)}, \quad (6)$$

where  $P$  stands for the principal value and  $E'$  is the energy where  $V(E = E', r)$  is known [26, 27, 28]. This equation tells us that once the imaginary part of the potential at a certain radius is known as a function of the energy the real part can be calculated from the relation. Thus, we inserted the imaginary potentials extracted from the  $\chi^2$ -fitting into the  $W(E, r)$  of Eq.(6), computed the real potential using the relation, and compared the results with the real potentials extracted from the  $\chi^2$ -fitting. In so doing, since the potential values in the nuclear surface region are most significant in determining the cross section, we first evaluate a strong absorption radius( $R_S$ )[16, 24] defined as the apsidal distance on the Rutherford trajectory corresponding to the angular momentum  $L = L_{1/2}$ , where  $L_{1/2}$  is the angular momentum for which the  $S$ -matrix element has the magnitude  $|S_L| = \sqrt{1/2}$ . Here, we used non-integer  $L_{1/2}$  values at which  $|S_L| = \sqrt{1/2}$ , following Ref. [16]. The  $L_{1/2}$  values thus obtained are listed in Table 1. The strong absorption radius parameter ( $r_S = R_S/A^{1/3}$ ) computed from these  $L_{1/2}$  values are also listed in Table 1 and plotted in Fig. 3(a) as a function of the pion energy. The  $r_S$  becomes as large as 1.6 fm near the  $\Delta$ -resonance region and about 1.1 fm at  $E \approx 400 - 500$  MeV. Note that Satchler's strong absorption radius parameters were also roughly around 1.5 fm near the  $\Delta$ -resonance energy [16]. To compare the values of the real and imaginary parts of the potentials at a certain radius, we took  $r = 1.5A^{1/3}$  fm in Eq. (6), which is close to a strong absorption radius near the  $\Delta$ -resonance energy.

In Fig. 4 is plotted by the solid circles the extracted real and imaginary parts of the potentials evaluated at  $r = 1.5A^{1/3}$  fm as a function of the energy. We could roughly fit

the solid circles in Fig. 4(b) by the sum of a Gaussian function and a constant of the form

$$W(E, r) = W_0 \exp\left(-\left(\frac{E - E_0}{\Delta E}\right)^2\right) + W_1, \quad (7)$$

where  $W_0$ ,  $E_0$ ,  $\Delta E$ , and  $W_1$  were found to be -13.9, 220, 110, and -3.34 MeV, respectively. The  $W(E, r)$  in Eq. (7) with these parameters is plotted by the curve in Fig. 4(b). We then inserted Eq. (7) into Eq. (6), chose the value of  $E'$  in Eq. (6) as 500 MeV, carried out the integral over the energy, and obtained the real part,  $V(E, r)$ . The resulting  $V(E, r)$  is plotted by the curve in Fig. 4(a), which roughly fits the extracted real potentials (the solid circles). As mentioned earlier, at 230, 260 and 280 MeV both attractive and repulsive potentials could fit the cross section data equally well. But the  $V(E, r)$  calculated from the dispersion relation (the full curve) prefers repulsive potentials at these energies.

The dispersion relation is applied at other radii also from  $1.3A^{1/3}$  to  $2.0A^{1/3}$  fm. In this radial region the extracted imaginary potentials can be fitted by Eq. (7) (but with different values of  $W_0$ ,  $E_0$ ,  $\Delta E$ , and  $W_1$ , of course, for each energy) with  $E_0 \approx 205$  MeV on the average. The real potentials calculated from the dispersion relation in this radial region reproduce the extracted real potentials just as well as in Fig. 4(a), so the figures are not repeatedly shown here. But outside this radial region, the extracted imaginary potentials are not so well fitted by Eq. (7). Also, the extracted real potentials are somewhat more scattered around the real potential curves calculated from the dispersion relation. Thus, it seems that the extracted phenomenological local potentials are consistent with the dispersion relation in this outer surface region.

Here, we note that although we reproduce the cross sections quite well as shown in Figs. 1 and 2 and the extracted local potentials in the outer surface region are reasonably consistent with the dispersion relation, it still does not necessarily mean that the extracted potentials are the unique ones which can describe the data. Particularly the inner part of the potentials can be quite different, as will be seen in Section 3, because this method cannot well determine the potentials inside the nucleus due to the absorption in



the nuclear surface region in addition to the fact that we have assumed the Woods-Saxon form of the local potential.

However, an interesting feature obtained from the results is the broad peak in the imaginary potential as seen in Fig. 4(b). For  $1.3A^{1/3} \text{ fm} < r < 2.0A^{1/3} \text{ fm}$ , the peaks are located at  $E = E_0 \approx 205 \text{ MeV}$  on the average, which is near the  $\Delta$ -resonance energy, and the  $\Delta E$  of the peaks is about 110 MeV. The  $\Delta$ 's produced in nuclei can get absorbed via processes such as quasi-free decay or spreading [13, 14, 29, 30]. Such an absorption is reflected in the flux of the incident pion as the imaginary part of the local potential peaked at about  $E = E_0$ . The region where the  $\Delta$  decays in nuclei through the quasi-free channel and the spreading was studied [30]. It was shown that the quasi-free decay takes place at  $r \geq 1.6A^{1/3} \text{ fm}$  and the spreading at  $r \geq 0.9A^{1/3} \text{ fm}$ . Since the quasi-free decay is the dominant decay process over the spreading by a factor of roughly 2 [29, 30], the strong absorption radius near the  $\Delta$ -resonance energy is mainly determined by the region where the quasi-free decay takes place, which is as large as about  $1.6A^{1/3} \text{ fm}$ . Fig. 3(a) and Table 1 show just that the extracted strong absorption radius parameters near the  $\Delta$ -resonance are about 1.6 fm, consistent with the results of Ref. [30]. Here, we also remark that 1.59 times  $\pi R_S^2$  roughly reproduces the total cross section as plotted by the crosses in Fig. 3(b), *i.e.*,  $\sigma_T \approx 1.59\pi R_S^2$ , where  $R_S = r_S A^{1/3}$  with  $r_S$  being the strong absorption radius parameter plotted by the squares in Fig. 3(a).

### 3 Comparison with Local Potentials Equivalent to Kisslinger potential

In this Section we briefly describe the Krell-Ericson transformation method [20] closely following Johnson and Satchler [22], where it was extensively applied to both  $\pi^+$  and  $\pi^-$  scattered from various target nuclei at pion energies from 20 to 291 MeV. A detailed study of the resulting equivalent local potentials can be found there.

We return to the truncated Klein-Gordon equation in Eq. (1).  $\omega$  is now taken as

the total energy of the pion in the pion-nucleus center-of-mass system. These slightly different definitions of  $\omega$  do not make any significant difference in the values of  $\omega$  because the mass of the pion is very small compared to that of target nuclei. For the nuclear potential  $V_N$  in Eq. (1) the Kisslinger form [7] of the potential has been frequently used, which can be written as

$$V_N = \frac{(\hbar c)^2}{2\omega} \left[ q(r) + \vec{\nabla} \cdot \alpha(r) \vec{\nabla} \right], \quad (8)$$

where the first term  $q(r)$  is mainly due to the pion-nucleon  $S$ -wave interaction and the second term comes from the  $P$ -wave part.

By rewriting the pion distorted wave function  $\phi(\mathbf{r})$  in Eq. (1) as

$$\phi(\mathbf{r}) = P(r)\psi(\mathbf{r}) \quad (9)$$

with the Perey factor  $P(r) = [1 - \alpha(r)]^{-1/2}$ , one can get a Schrödinger equation for  $\psi(\mathbf{r})$ ,

$$\left[ -\frac{\hbar^2}{2\mu} \nabla^2 + U_L + V_C \right] \psi = E_{c.m.} \psi, \quad (10)$$

where  $\mu = \omega/c^2$  and  $E_{c.m.} = (\hbar k)^2/2\mu$ . Here,  $U_L$  is a local potential dependent only on  $r$  as follows:

$$U_L = U_1 + U_2 + U_3 + \Delta U_C \quad (11)$$

with

$$\begin{aligned} U_1 &= \frac{(\hbar c)^2}{2\omega} \frac{q(r)}{1 - \alpha(r)}, \\ U_2 &= -\frac{(\hbar c)^2}{2\omega} \frac{k^2 \alpha(r)}{1 - \alpha(r)}, \\ U_3 &= -\frac{(\hbar c)^2}{2\omega} \left[ \frac{\frac{1}{2} \nabla^2 \alpha(r)}{1 - \alpha(r)} + \left\{ \frac{\frac{1}{2} \nabla \alpha(r)}{1 - \alpha(r)} \right\}^2 \right], \\ \Delta U_C &= \frac{\alpha(r) V_C}{1 - \alpha(r)}. \end{aligned} \quad (12)$$

Thus if  $q(r)$  and  $\alpha(r)$  are given, the local potential  $U_L$ , exactly phase-shift equivalent to the Kisslinger potential, can be calculated. The expressions and parameters for  $q(r)$  and

$\alpha(r)$  for the system of  $\pi^- + {}^{12}\text{C}$  at 7 energies from 120 to 280 MeV are available from the work of Sternheim and Auerbach [25], where simple forms of  $q(r)$  and  $\alpha(r)$  are used:  $q(r) = b_0 k^2 \rho(r)$  and  $\alpha(r) = b_1 \rho(r)$  with  $\rho(r)$  being the target nuclear density. (Note that  $b_1$  here corresponds to  $c_0$  in the notation of Johnson and Satchler [22].) We have used "Fermi averaged parameters" for  $b_0$  and "Fitted parameters" for  $b_1$  as listed in Table I of Ref. [25]. The same parameter sets were used by Di Marzio and Amos to calculate approximate analytic pion distorted wave functions [31]. We took the  ${}^{12}\text{C}$  density from Ref. [31], which is consistent with Ref. [32].

The real and imaginary parts of  $U_L$  calculated with these parameters are plotted by the full curves in Figs. 5(a) and 5(b), respectively, for  $E = 120, 150, 230,$  and  $280$  MeV only. (For brevity, figures for 180 and 260 MeV are omitted.  $U_L$  for 200 MeV is shown in Fig. 6.) Both real and imaginary parts of  $U_L$  display a wiggly behaviour, as already observed in Refs. [21] and [22], but the wiggles disappear as the energy increases. The reason for the gradual disappearance of the wiggles at higher energies can be easily seen, when the Kisslinger potential is expressed in a simple form as in Refs. [25] and [31]. In Fig. 6, each term of  $U_L$  is plotted for two different pion energies; one below the  $\Delta$ -resonance, the other above the resonance. The real and imaginary parts are plotted by the full and broken curves, respectively. It is easily seen that  $U_2$  and  $U_3$  are the terms that characterize the shape of the summed local potential  $U_L$ .  $U_2$  determines the overall shape of  $U_L$  for both below and above the resonance, and  $U_3$  brings in more fluctuations, particularly below the resonance. As the energy increases the wiggles in all terms of  $U_L$  become less prominent. Such gradual disappearance of oscillatory behaviours of the real potential at higher energies was already observed in a model-independent Fourier-Bessel analysis of the pion potential by Friedman [33], who extracted the real potential by assuming the Woods-Saxon form for the imaginary potential. The same tendency of disappearance of wiggles at higher energies can be also seen from the figures in Refs. [21] and [22].

We can also see that the wiggles do not appear in the outer nuclear surface region, where the scattering is most sensitive to the potential. Thus, as the energy increases, the equivalent local potentials at large radii become more or less close to the form of a Woods-Saxon potential. In Fig. 5 we plotted by the broken curves the phenomenological Woods-Saxon potentials extracted in Section 2. At 230, 260 and 280 MeV the phenomenological local potentials are close to the equivalent local potentials  $U_L$  (the full curves) in the outer surface region. Especially, the imaginary parts at large radii are very close to each other. But at lower energies there are large discrepancies between the phenomenological Woods-Saxon potentials and the equivalent local potentials. Even the signs of the real potentials are opposite except for large radii at 120 MeV. (We may, however, remark that even the equivalent local potentials could have different signs of real potentials at smaller radii depending on the interaction parameters used as shown in Fig. 13 of Ref. [22], while they produce similar scattering cross sections, because the scattering is most sensitive to the potential at large radii.) As pointed out earlier, we can see from Fig. 4(a) that the real potentials at  $1.3A^{1/3} \text{ fm} < r < 2.0A^{1/3} \text{ fm}$  are repulsive only at the energies just above the  $\Delta$ -resonance. Thus, the dispersion relation calculations seem to require attractive potentials at energies below the  $\Delta$ -resonance in the outer surface region.

Also, although the equivalent local potentials are theoretically better founded, the phenomenological Woods-Saxon potentials reproduce the cross sections much better, as shown in Fig. 1. (The equivalent local potentials obtained here result in the same differential cross sections as in Figs. 1 and 2 of Ref. [25], so they are not repeated here.)

## 4 Summary

We assumed the Woods-Saxon form of phenomenological local potentials in solving a Schrödinger equation reduced from the Klein-Gordon equation and searched for the potential parameters. The calculated cross sections reproduced the experimental cross sections quite well in a wide range of energy. The real and imaginary parts of the phe-

phenomenological potentials in the outer nuclear surface region are found to satisfy the dispersion relation. The imaginary part of the phenomenological local potentials as a function of the energy has a peak near the  $\Delta$ -resonance energy due to the decay of the  $\Delta$ 's in the nuclear medium, which is reflected in the pion flux as absorption of the incident pion. The strong absorption radius ( $\approx 1.6A^{1/3}$  fm) in the  $\Delta$ -resonance region is found to be consistent with the previous studies of the region where the  $\Delta$  decays in the nuclear medium. But we again stress that the phenomenological local potentials obtained here are not necessarily unique. This method of calculating the pion cross sections may rather be taken as a simple way of taking into account the distortion effects in the DWBA or DWIA calculations with a relatively good accuracy as in Ref. [16]. It is well known that for high energy beams the distortion effects can be often treated by an eikonal approximation with so-called a distortion factor or an attenuation factor. Indeed, Table 1 shows that at higher energies the real part of the phenomenological local potential becomes much smaller than the imaginary part.

Very recently this approach to the treatment of the distortion effects has been applied to the  $^{12}\text{C}(\pi^+, K^+)_{\Lambda}^{12}\text{C}$  reaction, and the distorted wave functions of  $\pi^+$  and  $K^+$  calculated in this method have been successfully used in reproducing the hypernuclear production cross sections in DWIA [34]. Even if the distorted wave functions calculated in this way may not be accurate especially inside the nucleus, this simple method seems quite useful in dealing with the distortion effects in view of the fact that most of the cross sections are well reproduced.

## Acknowledgements

We are grateful to Professor T. Udagawa for his hospitality at the University of Texas

at Austin and for his careful reading the manuscript and helpful discussions. SWH owes thanks to Drs. H. W. Fearing and B. K. Jennings for their hospitality at TRIUMF and discussions and Professor B. C. Clark for sending some of the experimental data in numbers. This work was supported in part by the Ministry of Education of Korea (BSRI 98-2422) and by Korea Science and Engineering Foundation (951-0202-033-2).

## References

- [1] See, for example, review articles such as Hüfner J. 1975 Phys. Rep. **21**, 1; Thomas A. W. and Landau R. H. 1980 Phys. Rep. **58**, 121; Oset E., Toki H. and Weise W. 1982 Phys. Rep. **83**, 282.
- [2] Eisenberg J. M. and Koltun D. S. 1980 *Theory of Meson Interactions with Nuclei* (New York: John Wiley and Sons).
- [3] Eisenstein R. A. and Miller G. A. 1974 Comput. Phys. Commun., **8**, 130.
- [4] Stricker K., McManus H. and Carr J. A. 1979 Phys. Rev. **C19**, 929; Stricker K., Carr J. A. and McManus H. 1980 *ibid.* **C22**, 2043.
- [5] Eisenstein R. A. and Tabakin F. 1976 Comput. Phys. Commun., **12**, 237.
- [6] Landau R. H. 1982 Comput. Phys. Commun., **28**, 109.
- [7] Kisslinger L. S. 1955 Phys. Rev. **98**, 761.
- [8] Landau R. H. and Tabakin F. 1974 Nucl. Phys. **A231**, 445.
- [9] Johnson M. B. and Siciliano E. R. 1983 Phys. Rev. **C27**, 730; 1983 *ibid.* **C27**, 1647; Siciliano E. R., Cooper M. D., Johnson M. B. and Leitch M. J. 1986 Phys. Rev. **C34**, 267.
- [10] Junker K., Karapiperis T., and Kobayashi M. 1991 Phys. Rev. **C43**, 1991.

- [11] Arima M., Masutani K. and Seki R. 1991 Phys. Rev. **C44**, 415; 1993 *ibid.* **C48**, 2541(E); 1995 *ibid.* **C51**, 431.
- [12] Chen C. M., Ernst D. J. and Johnson M. 1993 Phys. Rev. **C47**, R9; 1993 *ibid.* **C48**, 841.
- [13] Hirata M., Lenz F. and Yazaki K. 1977 Ann. Phys. (N.Y.) **108**, 116;  
Hirata M., Koch J. H., Lenz F. and Moniz E. J. 1979 *ibid.* **120**, 205.
- [14] Karaoglu B. and Moniz E. J. 1986 Phys. Rev. **C33**, 974.
- [15] Körfggen B., Osterfeld F. and Udagawa T. 1994 Phys. Rev. **C50**, 1637.
- [16] Satchler G. R. 1992 Nucl. Phys. **A540**, 533.
- [17] Binon F. *et al.* 1970 Nucl. Phys. **B17**, 168.
- [18] Takahashi T. *et al.* 1995 Phys. Rev. **C51**, 2542.
- [19] Kahrmanis G. *et al.* 1997 Phys. Rev. **C55**, 2533.
- [20] Krell M. and Ericson T. E. O. 1969 Nucl. Phys. **B11**, 521.
- [21] Parija B. C. 1983 Phys. Rev. **C28**, 453.
- [22] Johnson M. B. and Satchler G. R. 1996 Ann. Phys. (N.Y.) **248**, 134.
- [23] Igo G. 1959 Phys. Rev. **115**, 1665.
- [24] Satchler G. R. 1983 *Direct Nuclear Reactions* (New York, Oxford Univ. Press).
- [25] Sternheim M. M. and Auerbach E. H. 1970 Phys. Rev. Lett. **25**, 1500.
- [26] Nagarajan M. A., Mahaux C. C. and Satchler G. R. 1985 Phys. Rev. Lett. **54**, 1136;  
Mahaux C., Ngo H. and Satchler G. R. 1986 Nucl. Phys. **A449**, 354; 1986 Nucl. Phys. **A456**, 134.

- [27] Fulton B. R., Baner D. W., Lilley J. S., Nagarajan M. A. and Thompson I. J. 1985 Phys. Lett. **162B**, 55.
- [28] Hong S. W., Udagawa T. and Tamura T. 1989 Nucl. Phys. **A491**, 492;  
Udagawa T., Tamura T. and Kim B. T. 1989 Phys. Rev. **C39**, 1840.
- [29] Udagawa T., Hong S. W. and Osterfeld F. 1990 Phys. Letts. **245B**, 1;  
Udagawa T., Oltmanns P., Osterfeld F. and Hong S. W. 1994 Phys, Rev. **C49**, 3162.
- [30] Udagawa T., Osterfeld F., Oltmanns P. and Hong S. W. 1991 *Proceedings of the 6th International Conference on Nuclear Reaction Mechanisms, edited by E. Gadioli* (Università degli Studi Milano) p.632.
- [31] Di Marzio F. and Amos K. 1985 Phys. Rev. **C 31**, 561.
- [32] de Jager C. W., de Vries H. and de Vries C. 1974 Atomic Data and Nuclear Data Tables **14**, 479.
- [33] Friedman E. 1983 Phys. Rev. **C28**, 1264.
- [34] Hong S. W., Kim B. T., Lee D. H. and Ryu C. Y. 1999 J. Korean Phys. Soc. **34** 9.



Table 1: The  $\pi^- + {}^{12}\text{C}$  phenomenological local optical potential parameters obtained from the  $\chi^2$ -fitting. The parameters are fixed such that they can reproduce not only differential elastic cross sections but also total elastic ( $\sigma_E$ ), reaction ( $\sigma_R$ ) and total ( $\sigma_T$ ) cross sections at all energies except for 400 and 500 MeV, where only differential cross sections are available. The radius and/or diffuseness parameters fixed during the search are underlined. The extracted  $L_{1/2}$  and strong absorption radius parameters are also listed at each energy. In computing the  $\chi^2$ -values for  $E = 486, 584, 663$  and  $766$  MeV, only the systematic errors of the experimental differential cross sections were taken for  $\Delta\sigma_{ex}^i$ .

$E$ (MeV)	$V$ (MeV)	$r_V$ (fm)	$a_V$ (fm)	$W$ (MeV)	$r_W$ (fm)	$a_W$ (fm)	$\chi^2$	$L_{1/2}$ ( $\hbar$ )	$r_S$ (fm)
120	-31.2	1.55	.257	-149.	<u>0.9</u>	.536	1.7	3.5	1.58
150	-54.0	1.20	.574	-103.	<u>1.0</u>	.566	8.9	4.1	1.58
180	-86.4	<u>0.9</u>	.553	-62.0	1.30	.455	2.7	4.7	1.59
200	-93.6	<u>0.9</u>	.571	-66.35	1.20	.4905	2.0	5.0	1.54
230	137.	<u>1.0</u>	.2156	-58.53	1.40	.3556	1.8	5.1	1.44
260	111.	<u>1.0</u>	.3136	-53.8	1.35	.3694	1.2	5.3	1.37
280	109.	<u>1.0</u>	.319	-46.74	1.35	.381	0.63	5.5	1.34
400	-39.4	1.12	<u>.4</u>	-59.8	<u>0.9</u>	.474	1.5	5.7	1.05
486	-22.0	1.124	<u>.4</u>	-70.3	<u>0.9</u>	<u>.4</u>	1.8	7.0	1.11
500	-31.8	1.05	<u>.4</u>	-53.8	<u>0.9</u>	.540	1.7	6.7	1.05
584	-12.4	1.20	.366	-69.8	<u>0.9</u>	.437	1.3	8.3	1.13
663	-4.90	1.37	.300	-64.0	0.965	.442	1.9	9.6	1.17
766	-4.11	1.40	.526	-60.3	<u>1.0</u>	.462	1.8	11.6	1.25

Figure 1: The calculated differential elastic cross sections (the full curves) are compared with the experimental data for  $\pi^- + {}^{12}\text{C}$ . The experimental data are taken from Ref. [17] for  $E = 120 - 280$  MeV. The data for  $E = 486, 584, 663$  and  $766$  MeV are from Ref. [18]. For  $E = 400$  and  $500$  MeV we used the data from Ref. [19].

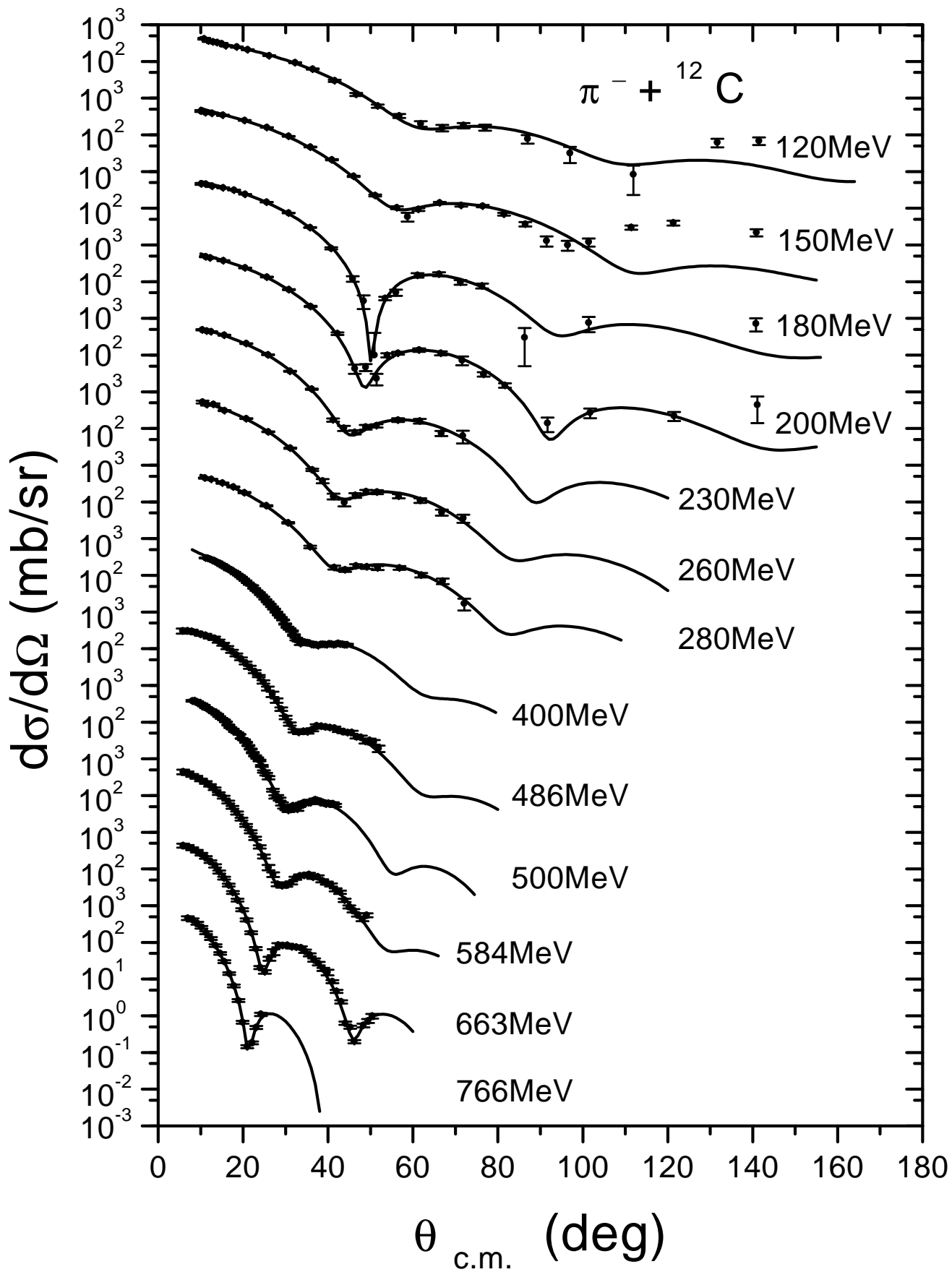
Figure 2: The calculated total elastic( $\sigma_E$ ), reaction( $\sigma_R$ ) and total( $\sigma_T$ ) cross sections denoted by the crosses are compared with the experimental cross sections for  $\pi^- + {}^{12}\text{C}$ . The data are from Refs. [17] and [18].

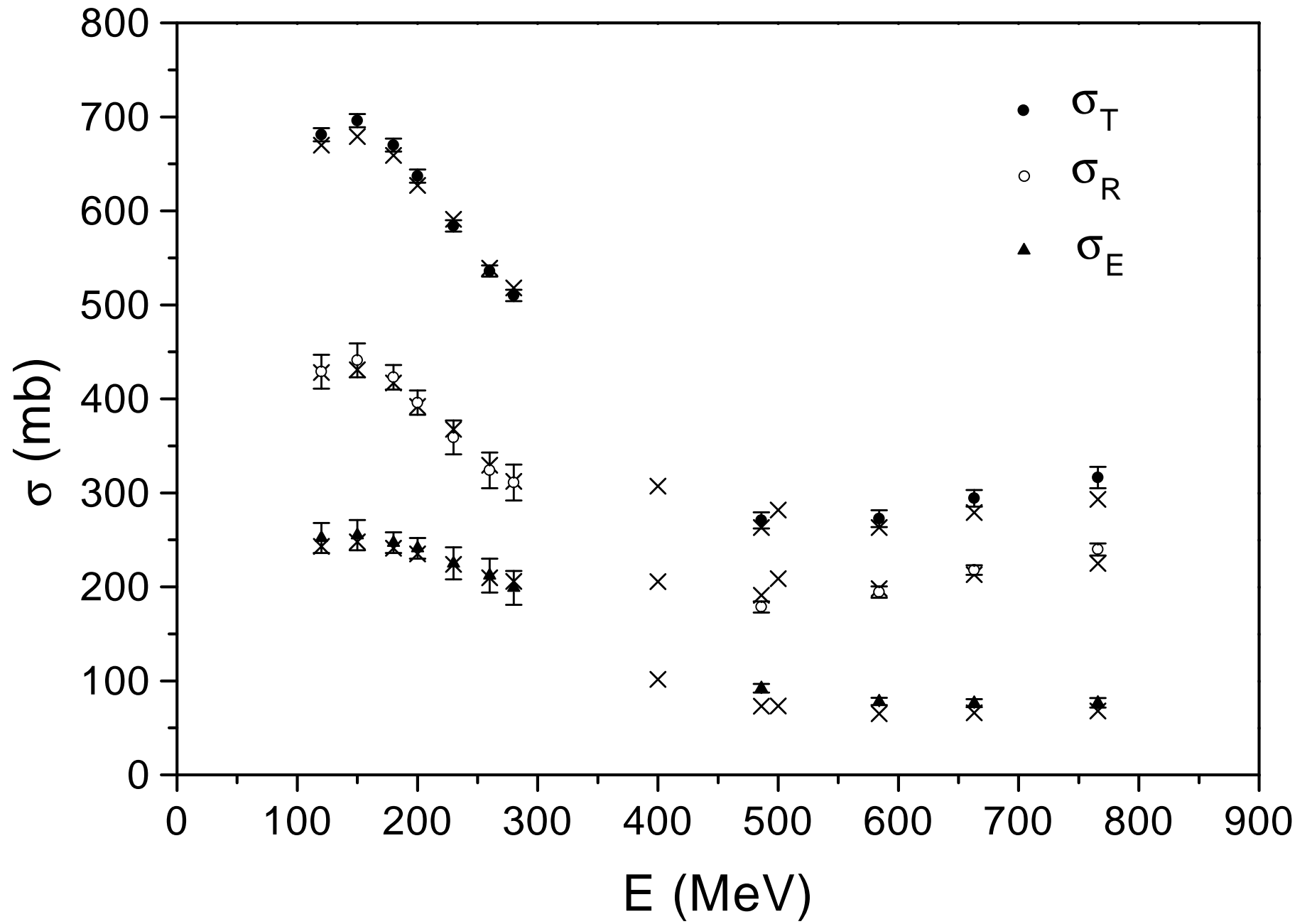
Figure 3: (a) The strong absorption radius parameters ( $r_S$ ) as a function of the incident pion energy. (b)  $1.59\pi R_S^2$  denoted by the crosses are compared with the experimental total cross sections. The data are taken from Refs. [17] and [18].

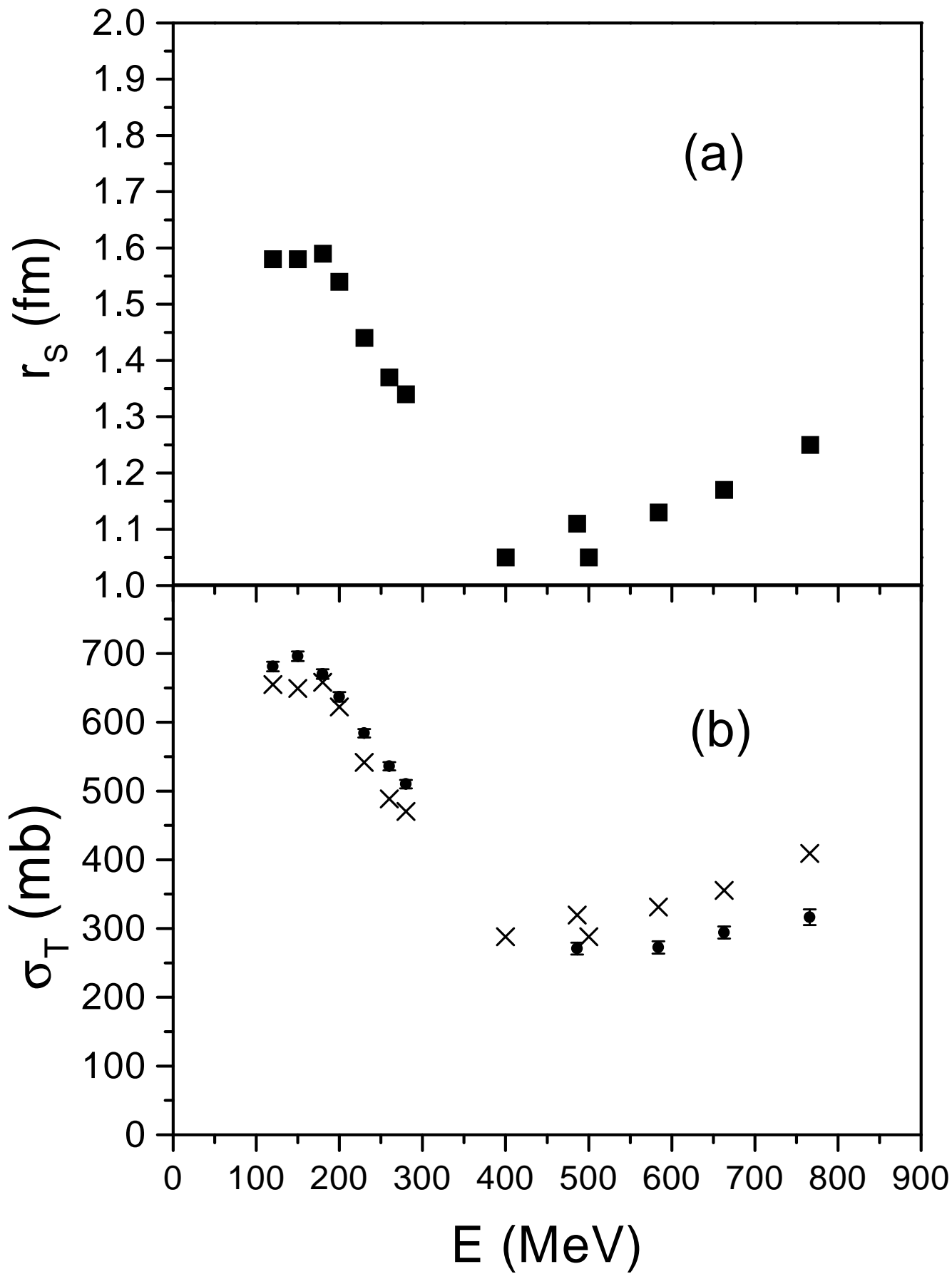
Figure 4: The real and imaginary potentials extracted from the  $\chi^2$ -fitting are computed at  $r = 1.5A^{1/3}$  fm and are plotted by the solid circles in (a) and (b), respectively. The extracted imaginary potentials (the solid circles in (b)) are fitted by the curve as explained in the text. The curve in (a) is the real potential calculated from the dispersion relation.

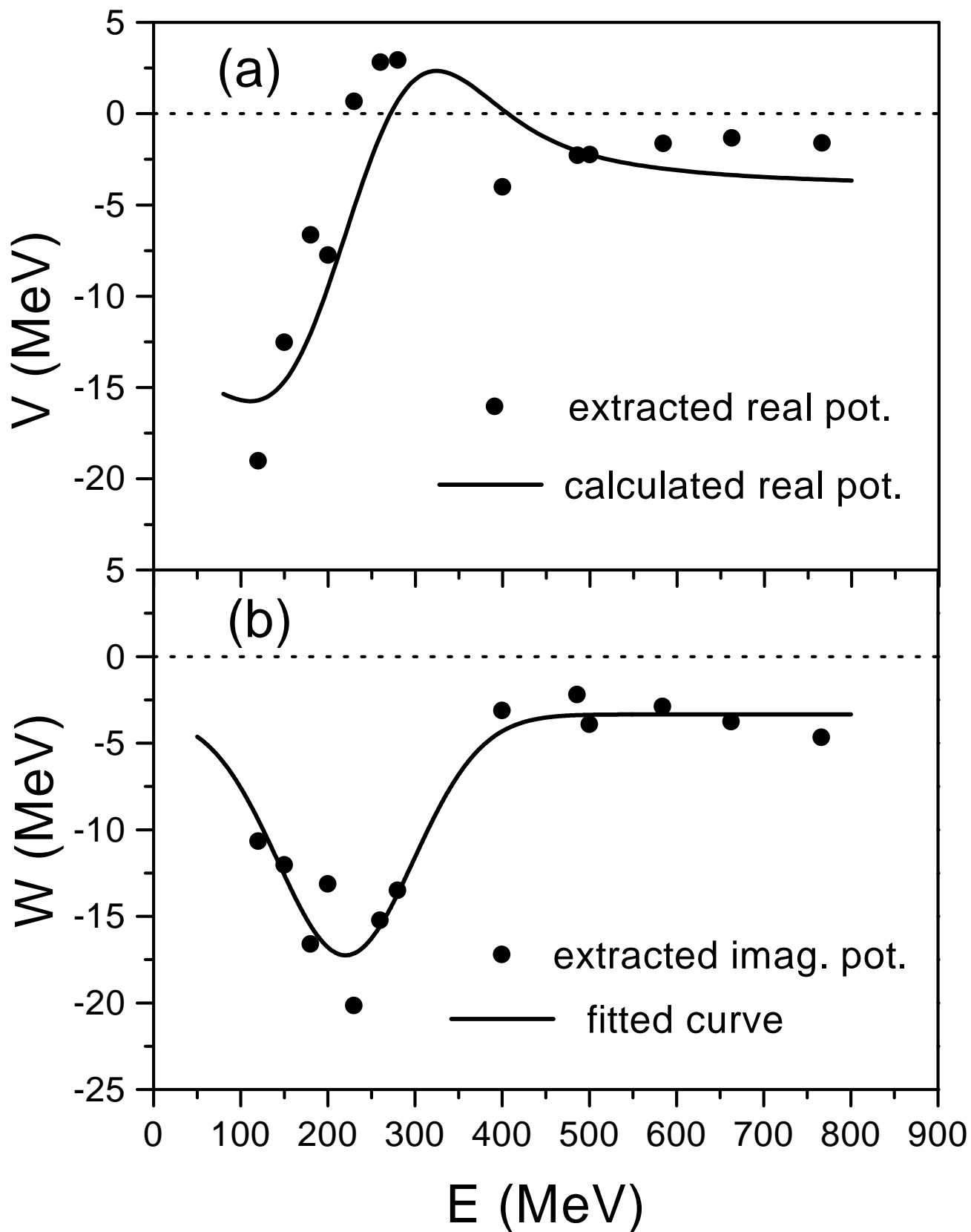
Figure 5: The local potentials  $U_L$  exactly phase-shift equivalent to Kisslinger potential calculated by using the Krell-Ericson transformation for  $\pi^- + {}^{12}\text{C}$  system for pion energies from 120 to 280 MeV are plotted by the full curves. (The potentials for 180, 200, and 260 MeV are not shown here for brevity.) The broken curves are the phenomenological Woods-Saxon potentials. The real and imaginary parts of the potentials are plotted in the columns (a) and (b), respectively.

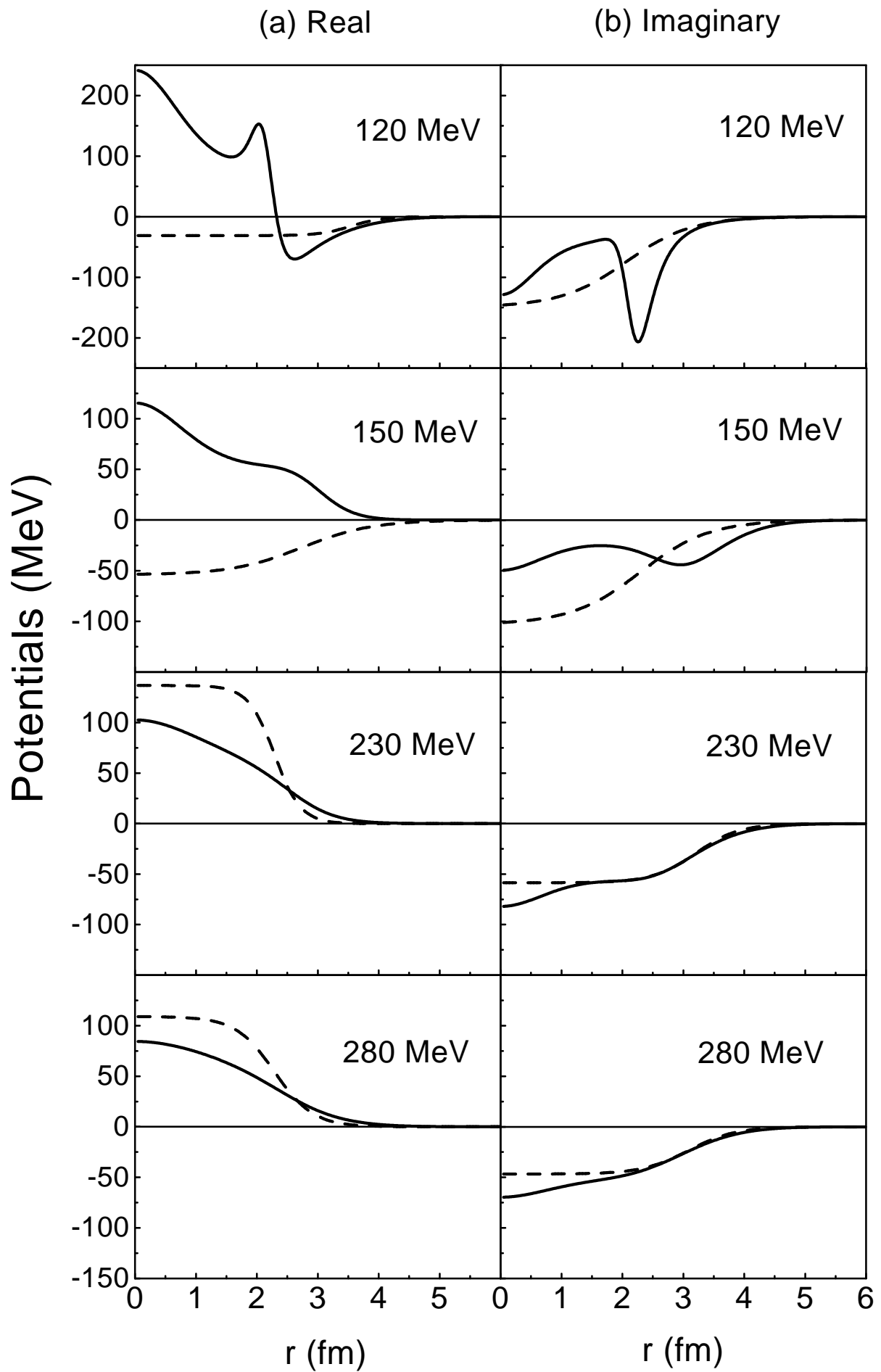
Figure 6: The  $U_1, U_2, U_3$ , and  $\Delta U_C$  components and the summed local potential  $U_L$  at 120 and 200 MeV are shown in column (a) and (b), respectively. The full and broken curves denote the real and imaginary parts, respectively.











(a) 120 MeV

(b) 200 MeV

